Bifunctional alloys for the electroreduction of CO_2 and CO

Heine A.Hansen[a], Chuan Shi[a], Adam C. Lausche[b], Andrew A. Peterson[a], Jens K. Nørskov[a,b]

[a]) SUNCAT Center for Interface Science and Catalysis, Department of Chemical Engineering, Stanford University, Stanford, CA 94305, USA.
[b]) SUNCAT Center for Interface Science and Catalysis, SLAC National Accelerator Laboratory, 2575 Sand Hill Road, Menlo Park, CA 94025, USA

Definition of Formation Energies

We have defined the formation energy of COOH*, E_{COOH}, as the DFT energy of the reaction[1]

$$CO_2(g) + * + \frac{1}{2} H_2(g) \rightarrow COOH^*.$$

The formation energy of CO*, E_{CO}, is the reaction energy for CO desorption[1,2]

$$CO(g) + * \rightarrow CO^*.$$

We define formation energies including adsorbate stabilization due to the solvent as[1]

$$E_{COOH(solv)} = E_{COOH} - 0.25 \text{ eV and } E_{CO(solv)} = E_{CO} - 0.1 \text{ eV}$$

The formation energy of CHO*, E_{CHO}, is calculated as the reaction energy of[2,3]

$$C + H_2O(g) + * \rightarrow CHO^* + \frac{1}{2} H_2(g),$$

where C is carbon in graphene. With the RPBE functional

$$C + H_2O(g) \rightarrow CO(g) + H_2(g)$$

has the reaction energy $E_{CO(g)}$=1.75 eV,[3] which allows calculation of E_{CHO} without explicit calculation of graphene. If

$$CO(g) + * + \frac{1}{2} H_2(g) \rightarrow CHO^*$$

has reaction energy ΔE_9, then $E_{CHO} = E_{CO(g)} + \Delta E_9$. The formation energy of OH*, E_{OH}, is defined using H_2O and H_2 as reference[2,3]

$$H_2O(g) + * \rightarrow OH^* + \frac{1}{2} H_2(g).$$

The formation energy of OCHO* is defined using CO_2 and H_2 as reference

$CO_2(g) + * + \frac{1}{2} H_2(g) \rightarrow OCHO^*$.

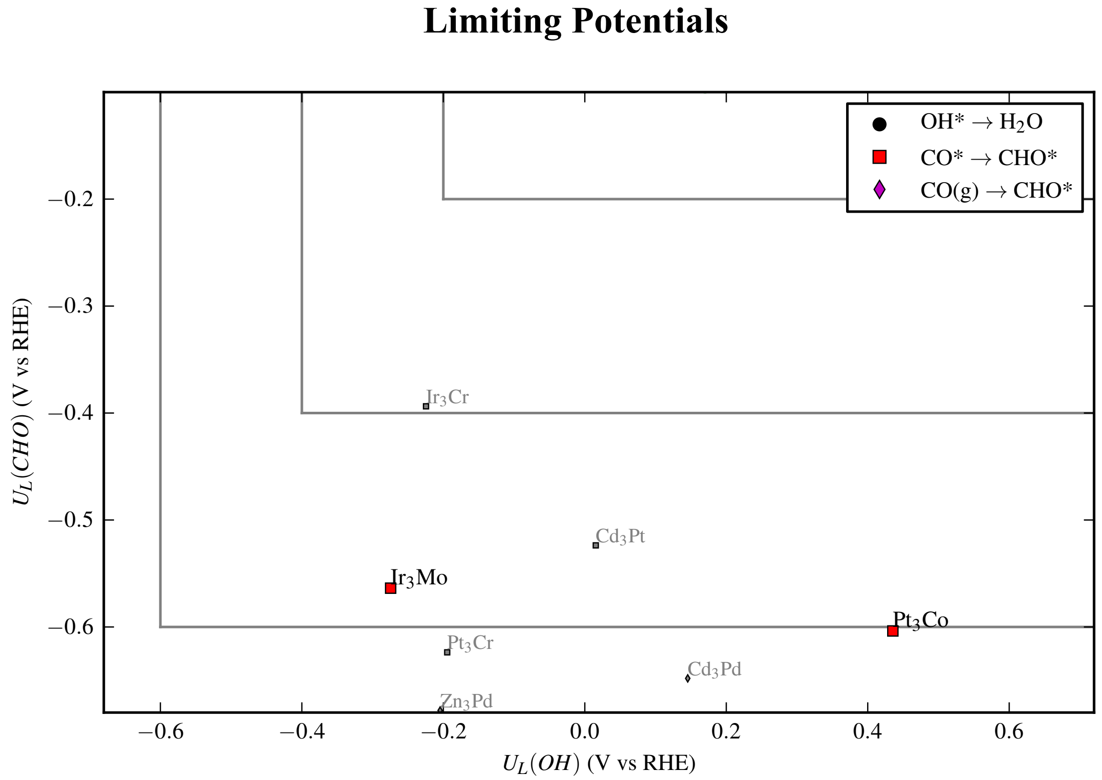

Figure S1: CO reduction on (111) facets approximated by the limiting potentials for OH removal and CHO formation. The potential limiting step is indicated in the legend. Alloys unstable at 0 V vs RHE and pH 7 are shown in gray with smaller symbols.

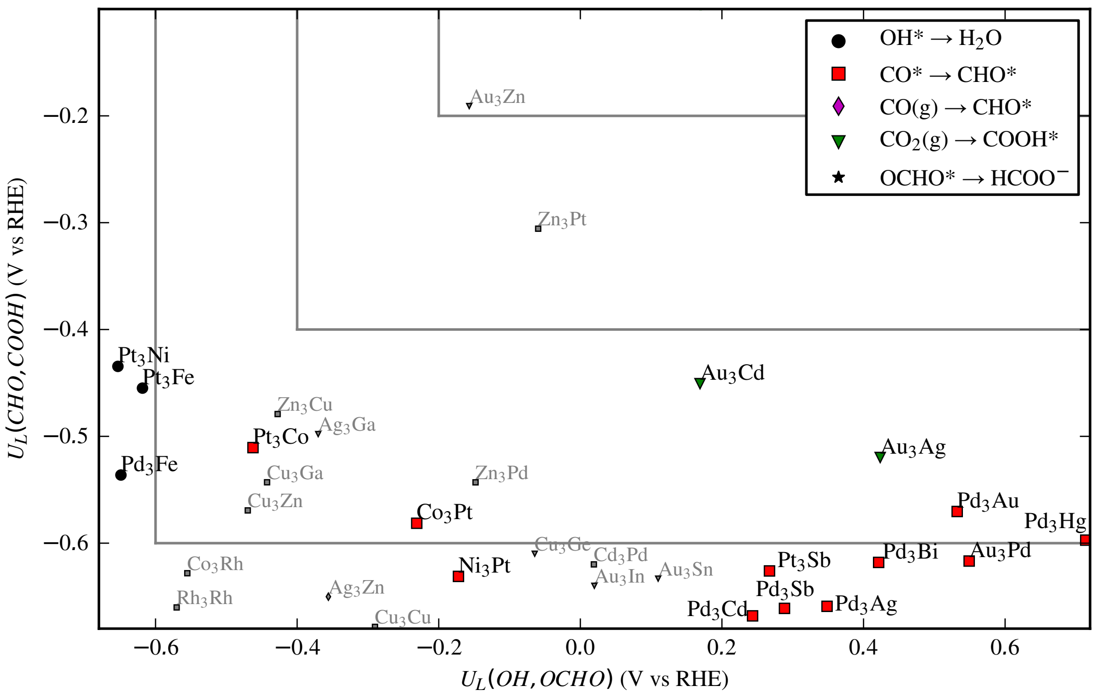

Figure S2: CO_2 reduction on (211) facets approximated by the limiting potentials for OH and OCHO removal and CHO and COOH formation. The potential limiting step is indicated. Alloys unstable at 0 V vs RHE and pH 7 are shown in gray with smaller symbols.

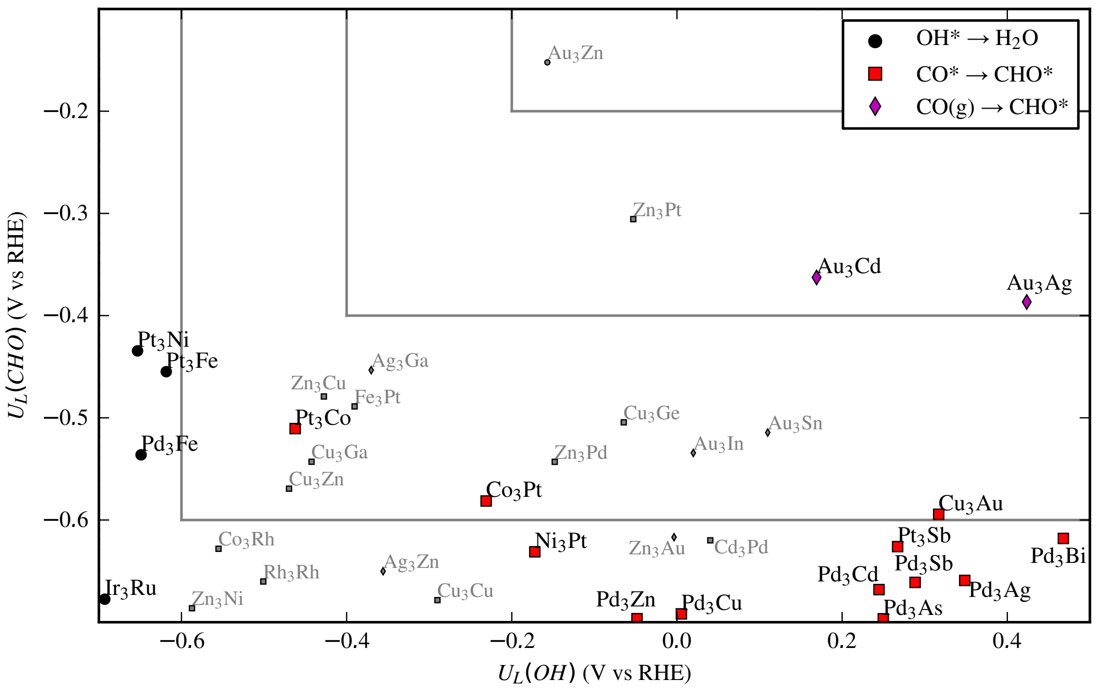

Figure S3: CO reduction on (211) facets approximated by the limiting potentials for

CHO formation and OH removal. The potential limiting step is indicated. Alloys unstable at 0 V vs RHE and pH 7 are shown in gray with smaller symbols.

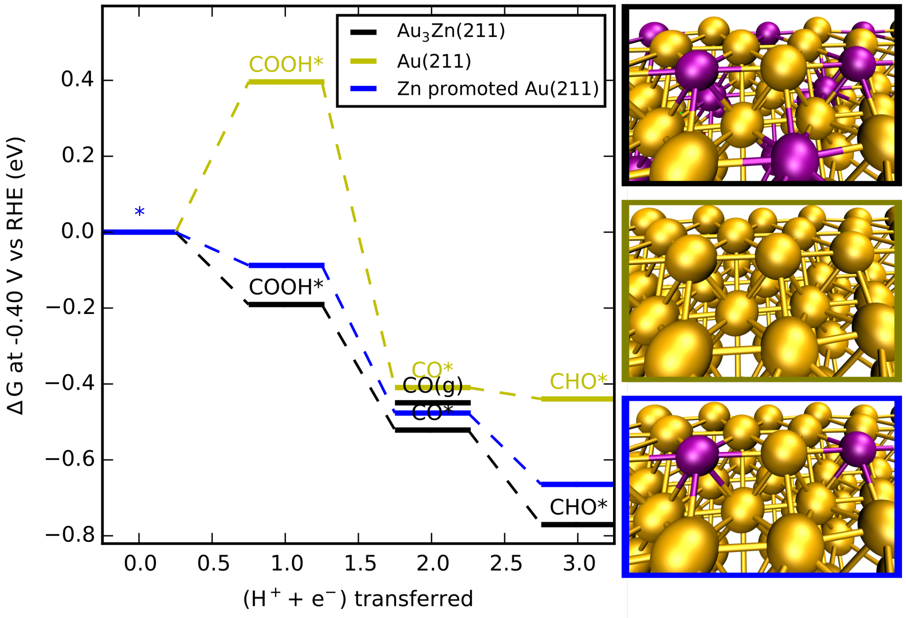

Figure S4: Free energy diagram for the initial reduction of CO_2 to CO and CHO* on Au_3Zn, Zn promoted Au and Au(211) at room temperature. Atomic structures are shown to the right. The free energy of CO(g) is shown at 1 atmosphere CO partial pressure.

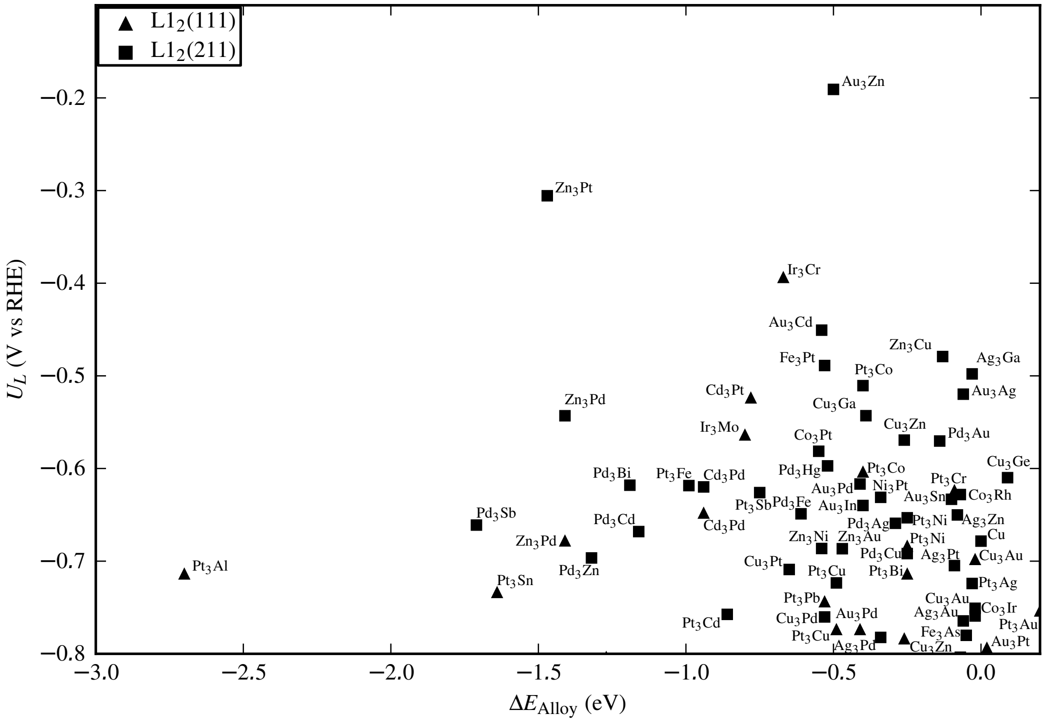

Figure S5: The limiting potential for CO reduction on (211) and (111) facets versus the alloy formation energy per formula unit of the $L1_2$ alloy.

Segregation

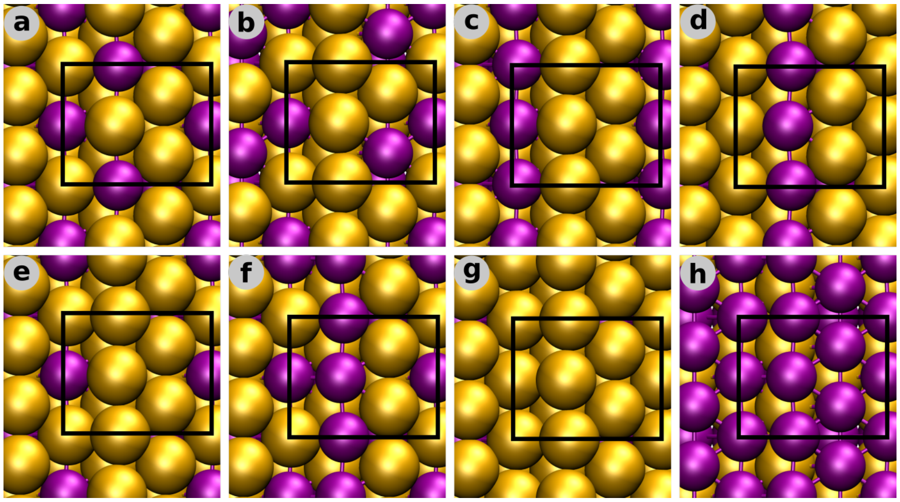

Figure S6: Atomic structures of (211) facets. (a) Stoichiometric A_3B(211) with AB termination. (b) + (c) Surfaces with A atoms along the step edge created from the stoichiometric surface by short-range exchange with atoms at the nearby terrace. (d) Surface with B atoms along the step edge created by short-range exchange with atoms at the terrace. (e)+(f) Surfaces with A and B at the step edge created by long range exchange of step atoms leaving the terrace unchanged. (g)+(f) Surfaces completely covered by A and B respectively.

The AB terminated A_3B(211) facet contains 4 A atoms and 2 B atoms as shown in Figure S6(a). Segregation energies are calculated from slab calculations based on the reactions below.

Swapping B atom at step edge with A atom at nearby terrace

$A_{(e)}B_{(e)}A_{3(t)}B_{(t)} \rightarrow A_{2(e)}A_{2(t)}B_{2(t)}$

where (e) and (t) subscripts denotes atoms at step and terrace respectively. In the final state the two possible locations of the swapped B atom are shown in figure S6(b)-(c). Swapping A atom at the step edge with the B atom at the nearby terrace results in the final state shown in figure S6(d)

$A_{(e)}B_{(e)}A_{3(t)}B_{(t)} \rightarrow B_{2(e)}A_{4(t)}$

The above processes conserve the stoichiometry of the simulation cell. We also consider phase separation along the step resulting in separate domains with either A or B atoms along the step edges as shown in figure S6(e)-(f).

$$A_{(e)}B_{(e)}A_{3(t)}B_{(t)} \rightarrow \tfrac{1}{2}\, A_{2(e)}A_{2(t)}B_{2(t)} + \tfrac{1}{2}\, B_{2(e)}A_{4(t)}$$

Finally, we consider complete phase separation on steps and terraces resulting in final states shown in Figures S6(g)-(h)

$$A_{(e)}B_{(e)}A_{3(t)}B_{(t)} \rightarrow 2/3\ A_{2(e)}A_{4(t)} + 1/3\ B_{2(e)}B_{4(t)}$$

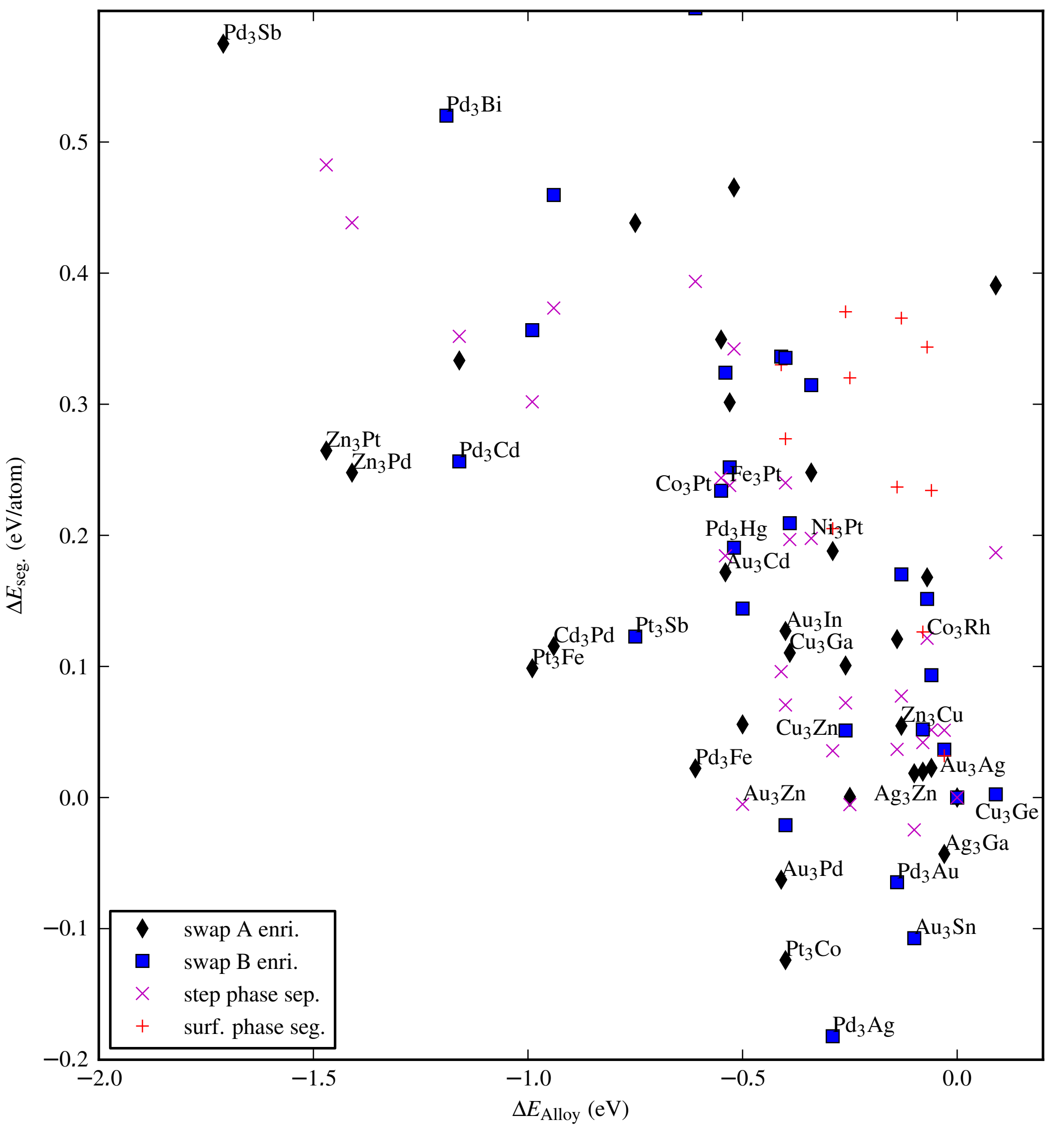

Figure S7: Segregation energies on (211) surfaces versus bulk alloy formation energies per formula unit.

CO reduction to CHO

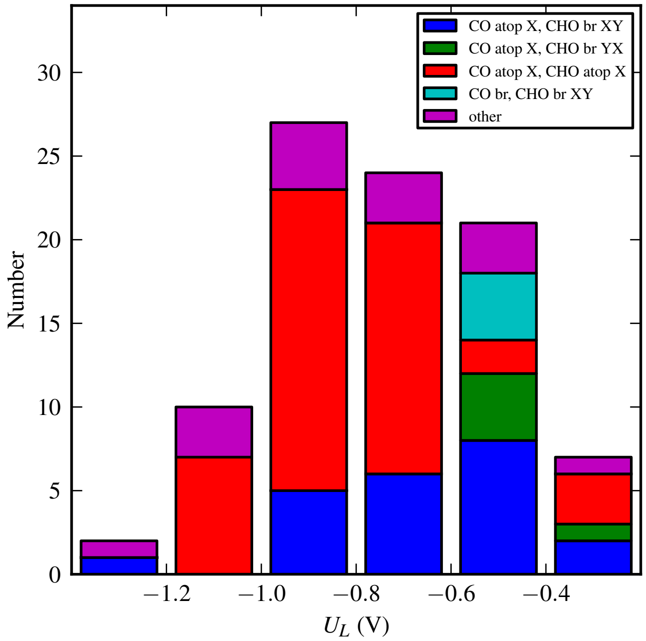

Figure S8: Histogram of CO and CHO configurations on (211) steps. "CO br" refers to CO adsorbed at a step bridge site through the C atom. "CO atop X" refers to CO adsorbed on an atom of type X at the step. "CHO br XY" refers to CHO adsorbed in a bridging position at the step with the C atom coordinated to an atom of type X and the O atom coordinated to an atom or type Y. The structures in figure 5(e)-(f) in the main text correspond to the class "CO atop X, CHO br XY". Only alloys with $E_{CO} < 0.05$ eV are included in this analysis.

References

1. H. A. Hansen, J. B. Varley, A. A. Peterson and J. K. Nørskov, *J. Phys. Chem. Lett.*, 2013, **4**, 388–392.
2. A. A. Peterson and J. K. Nørskov, *J. Phys. Chem. Lett.*, 2012, **3**, 251–258.
3. A. A. Peterson, F. Abild-Pedersen, F. Studt, J. Rossmeisl and J. K. Nørskov, *Energy Environ. Sci.*, 2010, **3**, 1311–1315.